Institut für Numerische Simulation
Rheinische Friedrich-Wilhelms-Universität Bonn

Wegelerstraße 6 • 53115 Bonn • Germany
phone +49 228 73-3427 • fax +49 228 73-7527
www.ins.uni-bonn.de

M. Griebel, J. Hamaekers, and F. Heber

A molecular dynamics study on the impact of defects and functionalization on the Young modulus of boron-nitride nanotubes

INS Preprint No. 0705

February 2009

A molecular dynamics study on the impact of defects and functionalization on the Young modulus of boron-nitride nanotubes

Michael Griebel, Jan Hamaekers, Frederik Heber*

Institute for Numerical Simulation,
Division of Numerical Simulation in the Natural and Engineering Sciences,
University of Bonn, Wegelerstraße 6, D-53115 Bonn, Germany.

Abstract

In this article, we examine the Young modulus of $(6, m)$ boron-nitride nanotubes with vacancy and functionalization defects. We employ molecular dynamics simulations using the Parrinello-Rahman approach. To this end, all systems are modeled with a reactive many-body bond order Tersoff-potential with parameters due to Matsunaga et al [1], which is able to accurately describe covalent bonding. We apply external stress to periodically repeated tubes in vacuum and derive stress-strain curves for various tensile loads at standard temperature and pressure. In addition to the Young modulus, we study visualized stress-per-atom snapshots of the simulation runs. Our results show that the decrease in Young modulus with increasing defect concentration is independent of the chirality of the tube for vacancy defects. Also, we observe that functionalization does not weaken the tube. There is even indication of a relative strengthening for armchair types.

Key words: molecular dynamics simulations, boron-nitride nanotubes, defects, functionalization, elastic moduli
PACS: 02.70.Ns, 62.20.de, 62.25.-g, 83.10.Rs.

1. Introduction

Nanotubes have attracted a lot of attention in the last decade due to their intriguing structural properties. Besides the well-known tubular structures made of

*Corresponding author. Tel.: +49 228 739847; fax: +49 228 737527.
Email address: heber@ins.uni-bonn.de (Frederik Heber)

carbon, there are now nanotubes made of a range of other materials. In particular, single- and multi-wall boron-nitride nanotubes (BN) can be produced with diameters comparable to those of carbon nanotubes, see [2] for an overview and references. Experimental studies [3] and semi-empirical calculations [4] show that BN nanotubes (BNNT) display a high Young modulus comparable at least to that of carbon nanotubes (CNT).

The stability at high temperature in air [5] and the high tensile strength of boron-nitride nanotubes suggest to use them for structural reinforcement of matrix materials. To this end, a functionalization of the embedded nanotube is essential to allow for cross-links to form between the nanotube and the ceramic material [6]. It has recently been shown that such a functionalization of the boron-nitride nanotube is possible with amine groups via ammonia plasma irradiation [7]. One question at hand is how this additional layer of nitrogen atoms or amine groups on the surface of the boron-nitride nanotube effects the tensile strength of the nanotube.

Additionally, defects play a critical role in fracture processes as they are always present, also in compound materials. Hence, measuring the strength of pristine material investigates only the possible upper limit of the Young modulus and the Poisson ratio, but not the magnitude encountered in real-life materials. These defects appear in a variety of forms: While single vacancy sites lead to point defects, line and layer defects are one- and two-dimensional defects typically found in periodic crystalline bulk materials. In nanotubes and related nanostructures these defects are compensated by specific patterns.

In this article, we investigate two types of scenarios that may weaken the tensile strength of a boron nitride nanotube: vacancy defects on the one hand and functionalization on the other hand. So far, Schmidt et al. [8] have studied various defects in BN nanotubes such as antisites, vacancies and carbon impurities, however not with regard to the Young modulus. Now, we investigate whether there is a diameter-dependent weakening of the nanotube. Furthermore, we are interested if the relation between the Young modulus and the defect concentration depends on the chirality of the tube.

To this end, we derive stress-strain curves of $(6, m)$ boron nitride nanotubes with vacancy defects and different degrees of functionalization by means of molecular dynamics simulations. We use standard temperature and pressure in the framework of the NPT-ensemble, similar to [9]. Note that we restrict ourselves to the study of diameter-dependent, not size-dependent effects, i. e. we fix the chirality number $n = 6$. The impact of a varying number n on the mechanical properties of nanotubes with intrinsic defects has already been studied elsewhere [10]. To model BNNTs, we use the Tersoff bond order potential [11], which is able to

describe covalent bonding in an accurate way. We apply an external stress tensor within the equations of motion of the Parrinello-Rahman-Nosé Lagrangian [12] to account for tensile loads. To model defects, we randomly remove a fixed number of atoms from the nanotube structure, whereas to model functionalization, we add a fixed number of nitrogen atoms on the surface of the nanotube structure at randomly picked boron sites. To investigate the impact of defects and functionalization on the Young modulus of BNNTs, we measure the stress-strain curve and derive the Young modulus for various setups with different chiralities for increasing defect concentrations and increasing degree of functionalization, respectively.

For carbon nanostructures Stone and Wales [13] proposed a 5-7-translation pattern for the compensation of defects. There, a C-C bond rotates in plane by 90°. In such a manner a doublet of adjacent pentagon/heptagon pairs is formed out of four connected hexagons (Stone-Wales defect). It has been shown that for carbon nanotubes under stress this kind of defect occurs prominently shortly before failure. Haskins et al [14] give a very good overview on the findings for carbon nanotubes. One may speculate that this process is different for boron-nitride nanotubes due to the antagonism of the two involved elements to form homo-elemental bonds [15]. It has been shown by density functional theory calculations that these 5-7-defects may form under high temperature and tensile stress [16]. However, there is also experimental evidence in [17] and numerical evidence in [18] speaking against the formation of pentagon/heptagon rings. Instead, quadragon/octagon rings are suggested. These however do require greater lattice distortions [16].

With our employed potential we investigate whether excluding or including homo-elemental bonds is important. In the first case there is only a repulsive force between two equal elements of either boron or nitride as, according to [1], they are not found in SiBN matrices. Here, we do not see any difference with the employed potential, whether we exclude or include homo-elemental bonds. This suggests that either the potential is not suitable for the simulation of Stone-Wales-defects – where homo-elemental bonds are present – or that these simply are not yet a relevant stress-relief scheme for defective nanotubes under initial strain, i. e. the nanotube cannot reduce site-specific stress by flipping bonds near the defect site in the aforementioned procedure under initial loading. We believe that the latter is the case and therefore Stone-Wales-defects are not considered here.

This article is organized as follows. In section 2 we outline the employed molecular dynamics method, the many-body potential and the stress-strain relationship. In section 3 we explain the experimental setup. The results are presented and discussed in section 4. Finally, we give some concluding remarks in section 5.

2. Method

All simulations are performed with our parallel software package TREMOLO, for further details see [19] and the references cited therein. Hence, in this section we only elaborate on the specifics of the employed canonical ensemble and its respective Hamiltonian and on how we obtain the Young modulus from the stress-strain relationship.

2.1. Molecular dynamics simulations

To switch from the usual Hamiltonian adapted to microcanonical NVE ensembles – i. e. constant number of particles (N), constant volume (V) and constant energy (E) –

$$\mathcal{H} = \tfrac{1}{2} \sum_{i=1}^{N} \frac{\vec{p}_{\vec{x}_i}^T \vec{p}_{\vec{x}_i}}{m_i} + U(\vec{x}_1, \ldots, \vec{x}_N) \tag{1}$$

to that for canonical NPT ensembles – i. e. constant number of particles (N), constant pressure (P) and constant temperature (T) – additional degrees of freedom have to be introduced according to Parrinello and Rahman [12]: we need a time-dependent matrix $\hat{h}$ which consists of the basis vectors of the simulation cell to re-scale the coordinates $\hat{\vec{s}}_i = \hat{h}^{-1}\vec{x}_i$, and a factor γ to re-scale the time $\overline{t} = \int_0^t \gamma(\tau) d\tau$ and thus also the velocities $\dot{\vec{x}}_i(\overline{t}) = \gamma \hat{h} \dot{\hat{\vec{s}}}_i(t)$. This way, there are nine degrees of freedom to control the pressure and one degree of freedom to control the temperature. We define the fictitious potentials $P_{\text{ext}} \det \hat{h}$ and $N_f k_B T \ln \gamma$ through the external pressure P_{ext} and the target temperature T, the system's number of degrees of freedom N_f and Boltzmann's constant k_B. Now, a so-called Parrinello-Rahman-Nosé Lagrangian can be postulated and an extended Hamiltonian

$$\begin{aligned} \mathcal{H} =& \tfrac{1}{2} \sum_{i=1}^{N} \frac{\vec{p}_{\vec{s}_i}^T G \vec{p}_{\vec{s}_i}}{m_i} + \tfrac{1}{2} \frac{\operatorname{tr}(p_h^T p_h)}{M_P} + \tfrac{1}{2} \frac{p_\eta^2}{M_T} \\ & + U(h, h\vec{s}_1, \ldots, h\vec{s}_N) + P_{\text{ext}} \det h + N_f k_b T \eta, \end{aligned} \tag{2}$$

can be derived, where $\eta := \ln \gamma(\overline{t})$, $\vec{s}_i(t) := \hat{\vec{s}}_i(\overline{t})$, $h(t) := \hat{h}(\overline{t})$, $G := h^T h$ and the constants M_P and M_T describe fictitious masses to control the time-scale of motion of the cell h and of the temperature. For details see [6], the references therein and the work of Nosé [20]. Note that there is an explicit dependency of V on the matrix h in the case of periodic boundary conditions, since atoms do not only interact with neighbors in the cell but also with those in translated images.

For the numerical solution of the equations of motion arising from (2) we have to employ a time-integration scheme. We use the "predictor-corrector" scheme based on Beeman's approach [21] with the modifications due to Refson [22].

Finally note that the physical energy $E_{\text{kin}} + U$ contained in (2) is not conserved in the NPT-ensemble, but the whole Hamiltonian (2), i. e. the sum of the physical energy, of the fictitious energy of the barostat and of the fictitious energy of the thermostat, remains constant over time.

2.2. Potential for boron and nitrogen

There are different empirical potential models available for covalent B-N systems, like the bond order potential of Tersoff [11] or the potential model of Marian and Gastreich [23]. In this work, we employ a Tersoff potential with the parameters of Matsunaga and Iwamoto from [1] where the potential parameters were fitted to data obtained from experiments and first principle methods. In particular, computed structural and elastic properties for various Si-B-N systems are in reasonable agreement with experimental results [1, 24]. Note that for the potential given in [1], the possibility of the formation of homo-elemental bonds between either boron or nitrogen is specifically excluded by modeling only a repulsive force, as these bonds are not seen in SiBN matrices. In contrast to that, i. e. to consider the effect of homo-elemental bonds as well, we adapt the potential of [1] to deal with B-B and N-N bonds, i. e. we include the corresponding attractive potential terms.

2.3. Stress-strain relationship

The stress-strain relationship provides the overall mechanical response of a material which is subjected to mechanical loading. To account for tensile loads, an additional symmetric external stress tensor Π_{ext} is used within the equations of motion. We may then increase or decrease each of the six independent components of Π_{ext} over a period of time and measure the induced internal stress tensor Π_{int} and the induced strain tensor ϵ. The strain ϵ is equal to the symmetric part $\frac{1}{2}(e^T + e)$ of the displacement matrix $e = hh_{\text{equi}}^{-1} - 1$, where h_{equi} is the symmetric equilibrated cell matrix h to which the system is constrained. This way, we generate stress-strain curves for tensile loads.

To determine the elastic constants, we assume that *Hooke's law*, which implies a linear stress-strain relationship, is fulfilled for small values of strain. For the stress tensor component $\Pi_{\alpha\beta}$ we obtain

$$\Pi_{\alpha\beta} = \frac{1}{\Omega} \frac{\partial E}{\partial \epsilon_{\alpha\beta}} \Big|_{\epsilon_{\alpha\beta}=0}, \tag{3}$$

where E is the system's total energy and Ω its volume. Then, the slope of the stress-strain curve under uniaxial tension is equal to the so-called Young modulus $Y_{\alpha\beta}$ which is defined as

$$Y_{\alpha\beta} = \frac{1}{\Omega} \frac{\partial^2 E}{\partial^2 \epsilon_{\alpha\beta}}\Big|_{\epsilon_{\alpha\beta}=0}. \tag{4}$$

The experimentally measured stress σ, that corresponds to $\Pi_{\alpha\beta}$, is defined as

$$\sigma = \frac{1}{A} \frac{dE}{d(L\epsilon_{\alpha\beta})} = \frac{F}{A}, \tag{5}$$

where E is the total energy, A the cross-section of the tube, F is the tensile force, L is the length and $d(L\epsilon)$ the change in length due to this force. Now, to compute the Young modulus $Y_{\alpha\beta}$ of a system, we simulate this system under uniaxial tensile load and obtain the discrete stress-strain curve. Then, due to Hooke's law, an approximation to the value $Y_{\alpha\beta}$ is computed by a least square linear regression. Note that, under the assumption that Hooke's law holds, equation (4) simplifies to $Y_{\alpha\beta} = \frac{\Pi_{\alpha\beta}}{\epsilon_{\alpha\beta}}$.

The calculated stress tensor Π however still depends on the volume Ω of the nanotube. Common convention [14] is to use the nantube's length times the area of an annulus with a diameter equal to that of the tube and the thickness equal to graphene, i. e. 3.4 Å, respectively. If there is more than one atom missing in the structure this procedure becomes questionable, as the vacancy naturally should decrease the local diameter. Also, the thickness of a BN sheet is not as well-defined as for graphene sheets due to the buckled nature of the structure which results from the different surface energies of the two involved elements. Instead, the thickness or interlayer distance, respectively, of hexagonal layered BN of 3.33 Å is commonly used [4]. We therefore employ a different gauging: To obtain the volume Ω, we sum up the van der Waals volumes of all atoms – 33.51 Å^3 for boron and 15.6 Å^3 for nitrogen. Thus, with increasing number of vacancy defects, the volume goes down slowly. Consequently, if the degree of functionalization increases, so does the volume.

3. Experimental Setup

In general, there is a periodic and a non-periodic way of setting up tensile load experiments with nanotubes in the computer. Here, we use the periodic setting, i. e. we simulate a tube of infinite length. As [25, 14] we also take the viewpoint

that defects are a length-dependent, statistical phenomenon and that the concentration of defects is the key parameter of interest in the prediction of mechanical properties.

Note that there are various types of vacancy defects. There exist divacancies – two defects on a plane orthogonal to the symmetry axis, but on opposite sides – which are also called disclustered defects in [14]. They often occur for CNTs when ion radiation of noble gases such as argon is present. Clustered defects on the other hand are adjacent vacancies. In the following, we do not take a specific type of defect into account. We merely intend to give a measure of the Young modulus against the defect *concentration* in order to derive bounds on how pure a BNNT has to be for use in later applications and to better understand if homogenization schemes should be applied after synthesis. As vacancy defects occur randomly, we presume that they take the form of both clustered and disclustered ones.

Our procedure is thus described by the following steps: First, we create nanotubes with chirality $(6,0)$, $(6,2)$, $(6,4)$, $(6,6)$, each having roughly 1000 atoms in case of vacancy defects and approximately 500-800 atoms in case of the functionalization setup. In both cases they possess a diameter between 5 and 8.5 Å. We use units cells of appropriate size and apply periodic boundary conditions, where we have set the lateral distance between the nanotube and its periodic images to about 20 Å. Second, we optimize each nanotube structure with respect to the periodic box length and the particle positions under standard temperature and pressure using the NPT-ensemble. Additionally, we constrain the box length changes to those in the direction of the tube's symmetry axis. We find the optimized bond length to be 1.47 Å which agrees well with the value 1.45 Å of the hexagonal BN lattice [10] and bond distances found elsewhere [26, 4]. Third, to create NTs with vacancy defects, 1, 5, 10, 20, 30, 40 and 50 atoms are randomly removed from the nanotube structure and the optimization is performed again. Here, we do not observe any mending of the created dangling bonds, i. e. we do not see any 5-7 or 4-8 defects appear. This is independent of whether the description of homo-elemental bonds is included in the potential or not. Finally, we use three different random seeds in the removal of a fixed number of atoms to obtain a statistical sample of the approximate error, which is given later in the figures.

On the other hand, to obtain functionalized nanotubes, we start from pristine optimized nanotube geometries and add nitrogen atoms at randomly picked boron sites. The nitrogen atoms act here as a model for ammonia [7] and nitric acid [27] which have also been used in experimental studies. To this end, we create eleven nanotube setups for each chirality with an increasing degree of functionalization

in steps of 10% from none to complete functionalization, see Figure 4 (left) for an illustration. Furthermore, we make samples with five different random seeds for each setup in order to obtain some statistical error bar for the approximate error of the method, see Figure 1 (right) and Figure 4 (left).

The simulations are then performed as follows: after 10.2 ps equilibration, an external stress tensor in the framework of the NPT-ensemble as described in section 2.3 is applied for 81.4 ps. Here, the atoms are constrained in their motion along the symmetry axis, i. e. only one of the six components of the external stress tensor which corresponds to the symmetry axis of the nanotube may increase. The stress rate is of course critical as we must allow for an adiabatic straining of the nanotube, i. e. after each stepwise increase of the stress the system should have sufficient time to equilibrate itself again. In [14] this alternation of application of stress and equilibration is done in step sizes of 1 ps. As we estimate the number of steps in [14] to be below 100, their overall run time is in the same order of magnitude as our overall run time, hence this implies a similar stress rate. The simulations were carried out to strains of 13%. In particular, we employ a rate of 0.5 femto Joule/ps to increase the external stress for this axial component. Note that this value has the unit of power, i. e. the amount of energy absorbed per time unit by the nanotube. To give the more common GPa/ps rate, we would have to factor in the volume. However, the volume is, as explained before, gauge-dependent whereas our value is not. Nevertheless, for comparison with practical experiments, we derived the GPa/ps rates: They were between 0.2 and 0.4 GPa/ps in our numerical experiments.

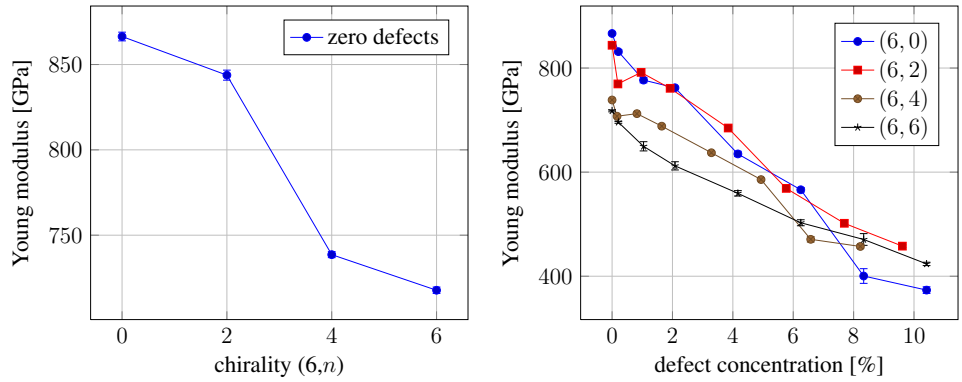

Figure 1: Comparison of the obtained Young modulus versus the chiralities $(6, 0)$, $(6, 2)$, $(6, 4)$ and $(6, 6)$ without and with vacancy defects. *Left*: Overall comparison of various chiralities without defects. *Right*: Young Moduls versus defect concentration for all chiralities.

4. Results

First of all, we consider the Young modulus of the pristine BNNT with different specific chiralities. The results are given in Figure 1 (left) for the pristine case, and in Figure 1 (right) for the case of increasing defect concentration. Here, the zigzag BNNT seems to be the strongest. Moon et al [28] have found no dependence of the Young modulus on chirality. Hernandez et al [29] have found a weak dependence on chirality, Verma et al [4] have found a strong dependence on chirality. Note that they both have observed the armchair type to be the strongest. We find this peculiar and not convincing due to the following consideration: In a spring model of the armchair case with atoms linked by mechanical springs, only two springs may work against the external stress in the direction of the symmetry axis while the third spring or bond, respectively, is orthogonal to it. In the zigzag case, however, all three springs may work against the external stress. Anyway, we find that our resulting moduli are perfectly in the regime of 0.7 – 1.2 TPa which was obtained in other numerical [29, 4] and practical [3, 30, 31] experiments. In Figure 2 we depict the stress per atom for the pristine nanotubes of different chiralities. It can be seen that the stress permeates through the nanotube quite homogeneously, which justifies our approach.

4.1. Vacancy defect study

In order to visualize the failure of BN nanotubes with a single defect, we show similar snapshots of the on-going simulation with stress-colored Van der Waals spheres. We briefly discuss the observations made for each chirality.

zig-zag In Figure 3(a) we see the defect site in blue, next to spheres colored also first blue, then green and finally red just before rupture occurs. This indicates that the defect site alone is exposed to a very small stress only. The rupture clearly occurs at the defect site with a distinct cut angle. The plane of the cut is slanted in direction of the symmetry axis. Such a rupture seems only possible for this chirality, as the cut plane for other chirality configurations would also have to slant continuously to the sides in a spiraling manner. Furthermore, we see a thinning of the remaining finite tube after rupture.

chiral In Figure 3(b) we observe that the clear cut for the $(6, 2)$ chirality configuration is not possible, instead we notice a thin thread of atoms in the final stage before failure and also a spiral twisting of the remainder of the structure. In Figure 3(c) we observe that the regular structure of chirality

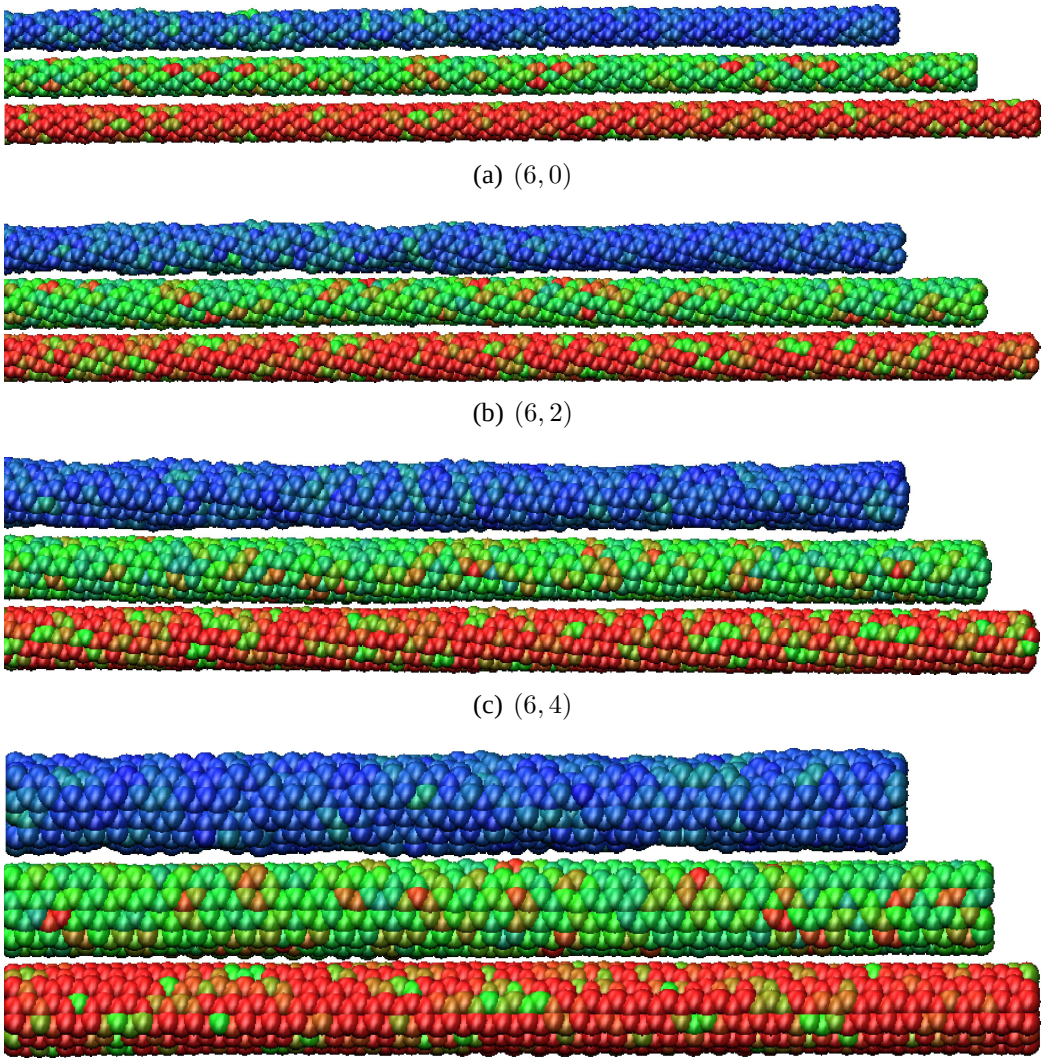

(a) $(6, 0)$

(b) $(6, 2)$

(c) $(6, 4)$

(d) $(6, 6)$

Figure 2: Defect-free stress-induced elongation of the discussed chiralities. Color indicates increasing stress per atom, from blue over green to red. From top to bottom: No strain at 10 ps, medium strain at 50 ps and final strain at 90 ps.

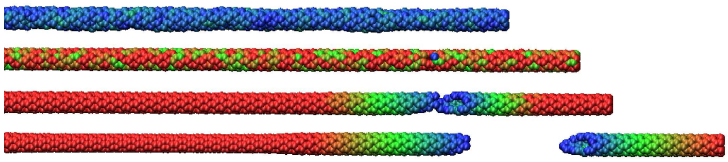

(a) $(6, 0)$

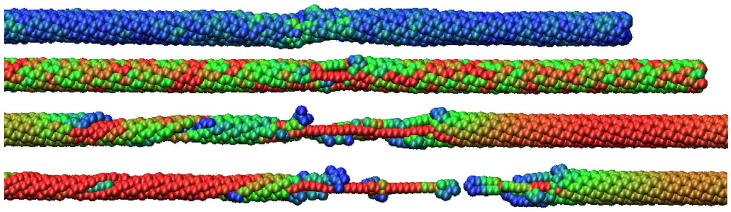

(b) $(6, 2)$

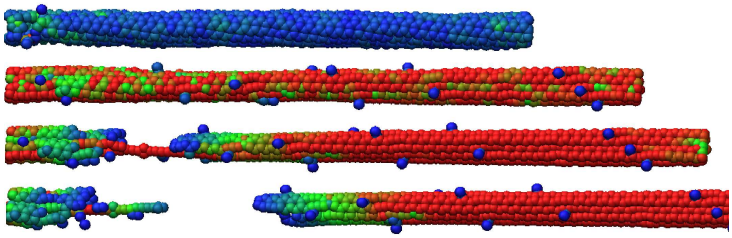

(c) $(6, 4)$

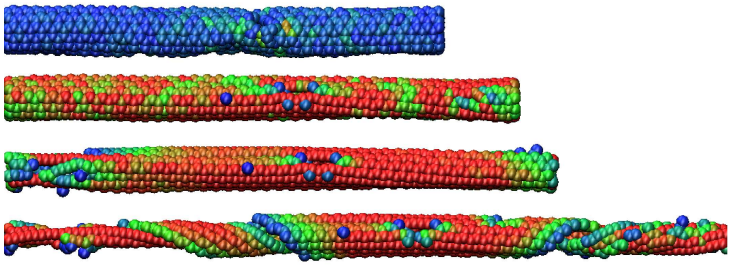

(d) $(6, 6)$

Figure 3: Stress-induced elongation and failure of the discussed chiralities with a single defect in the periodic cell. Color indicates increasing stress per atom, from blue over green to red. From top to bottom: No strain at 10 ps, strain before, at and after failure.

$(6,4)$ collapses after a certain amount of stress was applied. This can also be seen from the many spheres colored blue that are dispatched from the regular structure in the final stage. Such a behavior is surely dependent on the chiral angle, as also the $(6,4)$ chirality has the smallest Young modulus in the defect free configuration.

armchair In Figure 3(d) we notice that, already during the initial equilibration, the defect site has increased to a clustered defect. Furthermore, the hole in the nanotube structure and a subsequent buckling is clearly visible. Here, a helical shearing must occur for the bonds to break in such a fashion. This later on ends in a spiral rupture of the structure close to the defect position. It would be very interesting to see this kind of failure experimentally replicated, e. g. by inducing the defect with an AFM. Note that Haskins et al [14] saw the same spiral-tearing in a (10,5) carbon nanotube.

Altogether, we have heuristically seen that the chirality of the BNNT has an influence on the rupture process. While the zigzag configuration shows a clear cut plane, the armchair configuration exhibits a spiral rupture. Intermediate types either collapse with respect to their chiral structure shortly before failure or exhibit again a spiral rupture. However, all intermediate types show single strands during final stage, like pearls on a thread.

In Figure 1 (right) we depict the computed Young modulus versus the defect concentration. We see that the tensile-loaded capacity seems to diminish linearly with the number of defects. This can be explained by the local stress already induced by the defects, as the structure has to adapt to it with increased bond lengths. Note the green coloring of the Van der Waals spheres around the defect sites in the very first of each snapshot in Figure 3 which indicates this increase in stress. The decrease due to the volume gauging as explained before is negligible here.

4.2. Functionalization study

The findings from our numerical experiments with functionalized nanotubes are summarized in Figure 4 (right). We see a general decrease of the Young modulus to $2/3$ of that of the pristine nanotube. This is mostly a volume effect as our volume gauge depends on the number of atoms, which increases by functionalization up to approximately 1.23 relative to the pristine nanotube's volume. This decrease is in particular observed in case of the zigzag type. The chiral types show a slowing down of this volume trend towards full functionalization. The

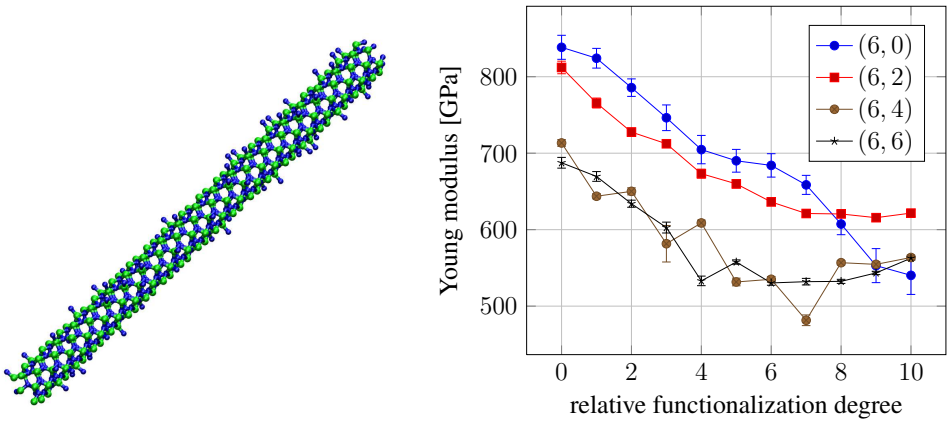

Figure 4: *Left*: Illustration of (6,0) BN nanotube, 30% functionalization with nitrogen in blue as model for NH_3. *Right*: Calculated Young modulus versus relative functionalization degree for (6,m) BN nanotubes.

behavior of the armchair configuration is especially interesting: Its modulus again increases significantly from 60% to 100% functionalization. This behavior could not be observed for the pure zigzag type.

Thus, we conclude that, in the context of the employed Tersoff potential, the bond strength in stress direction is *not* negatively affected by the functionalization. There even seems to be a strengthening of the bond structure in symmetry direction in the case of (near-)armchair configurations for full functionalization.

5. Discussion

We studied the behavior of the Young modulus of boron-nitride nanotubes in the framework of molecular dynamics simulations with the NPT-ensemble. Here, we considered two cases that bear particular significance on the proposed embedding in compound materials: vacancy defects and functionalization. We find a general, chirality-independent decrease of the tensile strength with increasing defect concentration. For functionalized boron-nitride nanotubes on the other hand, we see no significant decrease with increasing functionalization and there is even evidence of a chirality-dependent increase.

This research was funded by the Deutsche Forschungsgemeinschaft (DFG) in the framework of the priority program SPP1165.

References

[1] K. Matsunaga, Y. Iwamoto, Molecular dynamics study of atomic structure and diffusion behavior in amorphous silicon nitride containing boron, Journal of American Ceramics Society 84 (10) (2001) 2213–2219.

[2] M. Terrones, J. M. Homo-Herrera, E. Cruz-Silvia, F. López-Urías, E. Muñoz-Sandoval, J. J. Velázquez-Salazar, H. Terrones, Y. Bando, D. Golberg, Pure and doped boron nitride nanotubes, Materials Today 10 (5) (2007) 30–38.

[3] N. G. Chopra, A. Zettl, Measurement of the elastic modulus of a multi-wall boron nitride nanotube, Solid State Communications 105 (5) (1998) 297–300.

[4] V. Verma, V. K. Jindal, K. Dharamvir, Elastic moduli of a boron nitride nanotube, Nanotechnology 18 (2007) 435711.

[5] Y. Chen, J. Zou, S. J. Campbell, G. Le Caer, Boron nitride nanotubes: Pronounced resistance to oxidation, Applied Physics Letters 84 (2004) 2430–2432.

[6] M. Griebel, J. Hamaekers, Molecular dynamics simulations of boron-nitride nanotubes embedded in amorphous Si-B-N, Computational Materials Science 39 (3) (2007) 502–517.

[7] T. Ikuno, T. Sainsbury, D. Okawa, J. M. J. Frehet, A. Zettl, Amine-functionalized boron nitride nanotubes, Solid State Communications 142 (11) (2007) 643–646.

[8] T. M. Schmidt, R. J. Baierle, P. Piquini, A. Fazzio, Theoretical study of native defects in BN nanotubes, Physical Review B 67 (2003) 113407.

[9] M. Griebel, J. Hamaekers, Molecular dynamics simulations of the mechanical properties of polyethylene-carbon nanotube composites, in: M. Rieth, W. Schommers (Eds.), Handbook of Theoretical and Computational Nanotechnology, Vol. 9, American Scientific Publishers, 2006, Ch. 8, pp. 409–454.

[10] G. Y. Gou, B. C. Pan, L. Shi, Theoretical study of size-dependent properties of BN nanotubes with intrinsic defects, Physical Review B 76 (2007) 155414.

[11] J. Tersoff, New empirical approach for the structure and energy of covalent systems, Physical Review B 37 (1988) 6991–7000.

[12] M. Parrinello, A. Rahman, Polymorphic transitions in single crystals: A new molecular dynamics method, Journal of Applied Physics 52 (12) (1981) 7182–7190.

[13] A. J. Stone, D. J. Wales, Theoretical studies of icosahedral C-60 and some related species, Chemical Physics Letters 128 (5,6) (1986) 501–503.

[14] R. W. Haskins, R. S. Maier, R. M. Ebeling, C. P. Marsh, D. L. Majure, A. J. Bednar, C. R. Welch, B. C. Barker, D. T. Wu, Tight-binding molecular dynamics study of the role of defects on carbon nanotube moduli and failure, Journal of Chemical Physics 127 (2007) 074708.

[15] Y. Miyamoto, A. Rubio, S. Berber, M. Yoon, D. Tománek, Spectroscopic characterization of stone-wales defects in nanotubes, Physical Review B 69 (12) (2004) 121413.

[16] H. F. Bettinger, T. Dumitrică, G. E. Scuseria, B. I. Yakobson, Mechanically induced defects and strength of BN nanotubes, Physical Review B 65 (4) (2002) 041406.

[17] E. Bengu, L. D. Marks, Single-walled BN nanostructures, Physical Review Letters 86 (11) (2001) 2385–2387.

[18] X. Blase, A. De Vita, J. C. Charlier, R. Car, Frustration effects and microscopic growth mechanisms for BN nanotubes, Physical Review Letters 80 (8) (1998) 1666–1669.

[19] M. Griebel, S. Knapek, G. Zumbusch, Numerical Simulation in Molecular Dynamics, Springer, Berlin, Heidelberg, 2007.

[20] S. Nosé, A molecular dynamics method for simulations in the canonical ensemble, Molecular Physics 52 (2) (1984) 255–268.

[21] D. Beeman, Some multistep method for use in molecular-dynamics calculations, Journal of Computational Physics 20 (2) (1976) 130–139.

[22] D. Refson, Molecular-dynamics simulation of solid n-butane, Physica B & C 131 (1985) 256–266.

[23] C. M. Marian, M. Gastreich, J. D. Gale, Empirical two-body potential for solid silicon nitride, boron nitride, and borisilazane modifications, Physical Review B 62 (5) (2000) 3117–3124.

[24] K. Matsunaga, Y. Iwamoto, Y. Ikuhara, Atomic structure and diffusion in amorphous Si-B-C-N by moleculder dynamics simulation, Materials Transactions 43 (7) (2002) 1506–1511.

[25] M. Sammalkorpi, A. Krasheninnikov, A. Kuronen, K. Nordlund, K. Kaski, Mechanical properties of carbon nanotubes with vacancies and related defects, Physical Review B 70 (24) (2004) 245416.

[26] S. Guerini, V. Lemos, P. Piquini, Theoretical investigations of BN armchair and zigzag nanoarch surfaces, Nanotechnology 17 (2006) 556–560.

[27] B. Satishkumar, A. Govindaraj, E. Vogl, L. Basumallick, C. Rao, Oxide nanotubes prepared using carbon nanotubes as templates, Journal of Materials Research 12 (3) (1997) 604–606.

[28] W. H. Moon, H. J. Hwang, Molecular-dynamics simulation of structure and thermal behaviour of boron nitride nanotubes, Nanotechnology 15 (2004) 431–434.

[29] E. Hernández, C. Goze, A. Rubio, Elastic properties of single-wall nanotubes, Applied Physics A - Materials Science & Processing 68 (3) (1999) 287–292.

[30] A. P. Suryavanshi, M. F. Yu, J. G. Wen, C. C. Tang, Y. Bando, Elastic modulus and resonance behavior of boron nitride nanotubes, Applied Physics Letters 84 (14) (2004) 2527–2529.

[31] A. Bosak, J. Serrano, M. Krisch, K. Watanabe, T. Taniguchi, H. Kanda, Elasticity of hexagonal boron nitride: Inelastic x-ray scattering measurements, Physical Review B 73 (4) (2006) 041402.